


The influence of friction stir processing on the microstructure and properties of the AD31T alloy

A.E. Medvedev ¹ ✉, V.V. Atroshchenko², A.S. Selivanov², A.R. Bogdanov¹,
M.V. Gorbakov³, Y.V. Logachev², V.S. Lobachev², A.R. Sadrislamov²

¹ Ufa University of Science and Technology, Ufa, Russia

² LLC Attestation Center Svarka Tech Service, Ufa, Russia

³ LLC Krus-Zapad, Ufa, Russia

✉ medvedevandreyrf@gmail.com

Abstract. The effect of friction stir processing treatment (FSP) on the microstructure and physical and mechanical properties of an aluminum alloy of the Al-Fe-Mg-Si system (AD31T alloy) has been studied. In particular, the influence of various processing modes on the formation of structural and bulk defects in the stir zone (SZ) was studied. The optimal technological parameters that ensure the formation of a tool with a relatively homogeneous defect-free structure for a given tool geometry is a tool rotation speed of 1120 rpm at a tool linear speed of 200 mm/min. It is shown that an increase in the linear speed of the tool in the range of 50–200 mm/min leads to a decrease of the heat-affected zone (HAZ), a smaller size of volume defects in the SZ, and more uniform deformation. The microstructure analysis data is confirmed by the microhardness and electrical conductivity measurement values. It is shown that the decrease in the electrical conductivity in the SZ does not exceed 2 % of the electrical conductivity of the base material.

Keywords: FSP; Al-Mg-Fe-Si; aluminium alloy; fine-grained structure: microhardness; electrical conductivity

Citation: Medvedev AE, Atroshchenko VV, Selivanov AS, Bogdanov AR, Gorbakov MV, Logachev YV, Lobachev VS, Sadrislamov AR. The influence of friction stir processing on the microstructure and properties of the AD31T alloy. *Materials Physics and Mechanics*. 2023;51(4): 38-49. DOI: 10.18149/MPM.5142023_4.

Introduction

The aluminum in the modern industry plays a key role; aluminum production is one of the strategic directions in non-ferrous metallurgy [1]. Due to low density, high thermal conductivity, low electrical resistance, high ductility, corrosion resistance, good manufacturability, assimilation in metallurgical production, and a set of performance characteristics, aluminum alloys are the basic structural materials in the aerospace industry, construction, railway transport, automotive industry, and shipbuilding [2]. The application sphere of aluminum alloys is constantly expanding. The technologies of its production and processing are being improved - both new methods for obtaining aluminum and alloys based on it [3,4], as well as methods for obtaining products and prepacks from them do appear [5]. At the same time, tasks related to the development of new and the development of existing technologies are relevant for modern mechanical engineering [4]. Recently, the creation of

gradient structures in materials, including those based on aluminum, has been actively developed. The structure of such materials is characterized by a designed inhomogeneity, providing different properties in the material's volume [6]. The most common method for obtaining gradient structures is surface treatment, due to the relative availability of the process, many ways of providing the treatment and the readiness of the product at the output. One approach to surface treatment to obtain a gradient structure is friction processing. Friction processing includes several methods, such as friction stir welding, friction stir processing, radial friction welding, friction soldering, etc. [7]. The most common of the methods listed above is friction stir processing (FSP). Processing by FSP [5] is a technology aimed at modifying the structure and properties of the surface of materials in the solid phase. Its difference from traditional methods is the absence of melting, which can lead to oxidation and overburning of the metal [8], and a decrease in its strength properties [9]. Studies on FSP have shown that this method, in addition to creating permanent joints, is able to modify the surface layer of the processed material, providing a different level of properties. It has been shown that FSP with superposition of tracks on aluminum surface makes it possible to achieve a reduction in the average grain size to 100–200 nm on a relatively large area, reaching an ultrafine-grained (UFG) state [10–12]. The authors propose a similar approach as one that makes it possible to obtain large-sized products with an UFG structure of the near-surface layer. The authors of [13] claim a more than 20-fold decrease in the average grain size because of one pass of FSP, which led to an increase in the yield strength of the material by 2.4 times. FSP has also found its way to modify surface chemistry and create aluminum-based composites. For example, application of FSP makes it possible to introduce reinforcing particles into the near-surface layer of a material without the formation of a liquid phase [14]. At the same time, the FSP itself contributes to the strengthening of the treated area. Thus, a combined effect on the product surface is achieved, which is unattainable by other approaches [15–17]. However, the published scientific results often lack precise data regarding tool configuration or processing mode details. Only approximate ranges of values for the speeds of movement and rotation of the tool, and the general configuration of the tool are given [18–20]. For further work, the exact values of these parameters are necessary, because their non-observance is fraught with the appearance of volumetric defects in the weld material [17,21,22]. The objective of this study is to analyze the microstructure and properties of AD31T aluminum alloy processed by FSP for four modes and to provide the recommendations on the exact geometry of the welding tool and processing conditions. The modes are tested on a model aluminum alloy, and the optimal mode will subsequently be applied to other aluminum alloys of the Al-Fe-Si system.

Materials and Experimental Methods

As a research material, hot-rolled aluminum alloy plates of 10 mm thick and 200x200 mm in size were used. The plates were obtained in the "T" state which means quenching and natural aging of the plate. This resulted in the inhomogeneity of the structure – there are coarse grains near the surfaces of the samples and finer grains closer to the middle of the sample. The chemical composition of the commercially produced AD31T alloy is given in Table 1.

Table 1. Chemical composition of the AD31T alloy

Concentration of the element, wt. %						
Al	Si	Fe	Mg	Mn	Cu	Zn
Base material	0.410	0.390	0.390	≤0.035	≤0.035	≤0.035

The processing of the material was carried out on a vertical console milling machine FSS-400, adapted for FSP, in 4 different processing modes (Table 2). During FSP the shoulder penetration was 0.635 mm at a tool inclination angle of 3°. The tool dwelling time after

immersion is 10 sec. Each mode provides 1 tool pass. During the FSP, the temperature in the treatment area was monitored using a TESTO 868 thermal imager.

Table 2. FSP modes

Sample marking for the X-Ray control	Tool rotation speed, rpm	Tool linear speed, mm/min	Max. temperature of the tool, °C
205	1120	50	600
204		100	560
206		160	470
207		200	440

A sketch of the tool is shown in Fig. 1. The tool is made of steel grade 20X13 (the closest analogue is AISI 420). Before use, the tool is hardened, after which its hardness is 580 HB. Most authors do not disclose the details of the geometry of the stirring tool, however, the general recommendations for aluminum alloys are that the tool pin should be a tapered cone or a threaded one [16,22]. However, the production of the threaded tool is more expensive and complex, than the production of the tapered cone tool [23]. Further it will be demonstrated that the simple tapered cone shape of the tool can provide the defectless structure, without having a need for the threaded tool.

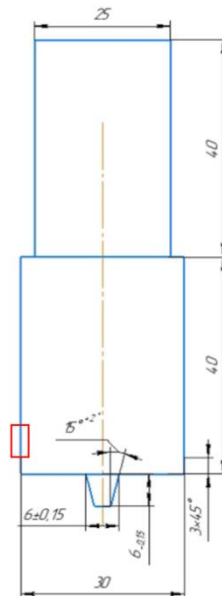


Fig. 1. Schematic of the stirring tool. Red rectangle indicates the location within the stirring tool, in which temperature measurements were conducted

X-ray control was carried out on the hardware-software complex of digital radiography "Tsifrakon". Microstructure studies were performed on an Olympus Q15OR optical microscope. For metallographic analysis, microsections were made, cut in the middle of the length of the treated zone in the direction perpendicular to the processing direction. Surface finishing was carried out in a 3 % hydrofluoric acid solution to reveal the macrostructure. Microhardness (HV) was evaluated by the Vickers method on a Buehler MicroMet 5101 instrument at a load of 1 N and a holding time under load of 10 s. The HV value was calculated using the Omnimet Imaging System software. Microhardness was measured on transverse sections of specimens along lines parallel to the surface of the original slab. The measurements were taken at the middle of the sample thickness, and $\frac{1}{4}$ of the height from the bottom and top surfaces of the slab. When measuring the microhardness of the stir zone, the line of

measurements passed through all sections of the cross section of the FSP sample at a measurement step of 0.5 mm (about 60 measurements per line). The specific electrical conductivity (ω) of the alloy samples was determined with a relative error of 2 % using a VE-27NTs/4-5 eddy current electrical conductivity meter according to ASTM E1004-09. The electrical conductivity value of the samples relative to annealed copper (International Annealed Copper Standard) was calculated using formula (1):

$$\text{IACS} = \omega_{\text{Al}} / \omega_{\text{Cu}} \times 100 [\%], \quad (1)$$

where ω_{Al} is the experimentally determined value of the electrical conductivity of the aluminum alloy sample, ω_{Cu} is the electrical conductivity of annealed copper, equal to 58 MSm/m. The electrical conductivity was measured at 10 points on a line located in the middle of the sample thickness.

Results and discussion

Stir zone (SZ) assessment. The overview of the treated samples and their X-ray control images are presented in Fig. 2.

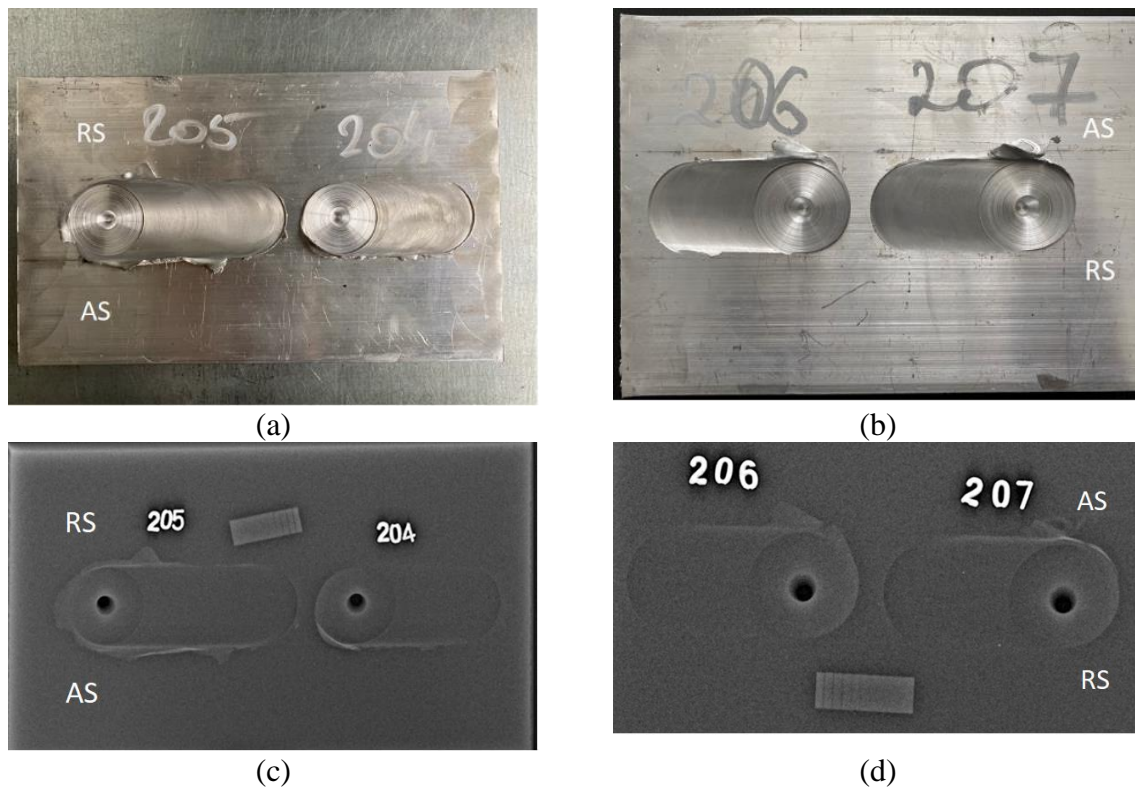


Fig. 2. The overview of the treated samples (a,b) and X-ray control images (c,d) of the samples 205, 204, 206 and 207. Advancing side (AS) and retreating side (RS) are indicated for each sample

X-ray quality control of the processed zone (PZ) showed that there are no macroscopic defects and discontinuities in the PZ in all four modes. The temperature in the PZ decreases with increasing linear speed of the tool (Table 2). With a decrease in the process temperature, both a decrease in the plasticity of the metal and an increase in the probability of the occurrence of bulk defects take place, as well as a decrease in the risks of melting, oxidation and the occurrence of recovery and recrystallization processes. Thus, the balance of the temperature should be maintained to prevent the abovementioned negative effects.

Macrostructure assessment. A stir zone (SZ), a thermomechanically affected zone (TMAZ), a heat-affected zone (HAZ) and a base material (BM) can be distinguished in the PZ. It should be noted that the width of the HAZ is small in all the samples, and only the SZ, HAZ, and BM are distinguished clearly. The width and geometry of the PZ (Fig. 3) directly depends on the parameters of energy input due to friction and is determined by two main parameters - the tool rotation speed and the linear speed of the tool movement. It should be noted that the TMAZ and HAZ decrease with an increase in the linear velocity of the tool (Table 2) and turned out to be the smallest for samples 206 and 207.

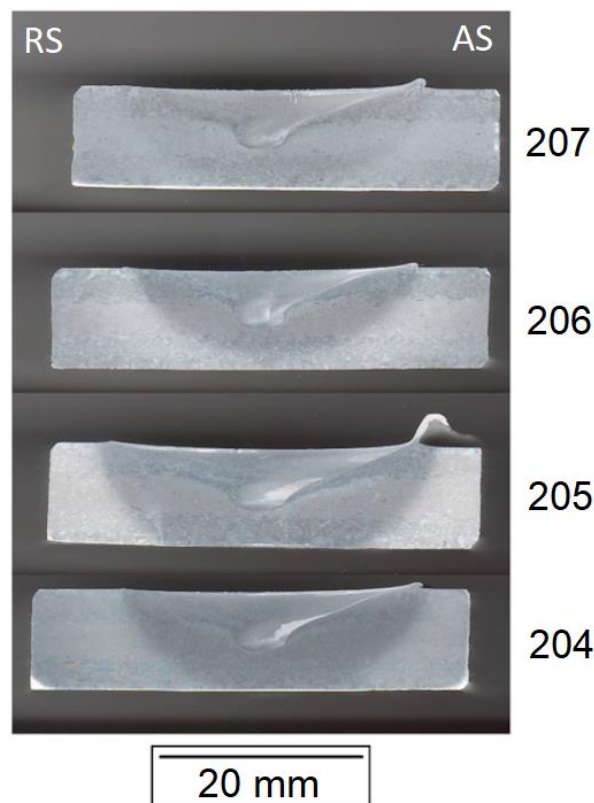


Fig. 3. The results of optical metallography of transverse sections of the studied samples

Figures 4 and 5 present the results of optical metallography of the structural features of the samples. Figure 4 shows the central part of the PZ of samples 204-207. The most uniform state of the material volume is observed in sample 207. Samples 205, 204 and 206 are characterized by the presence of volume defects in the central part of the SZ.

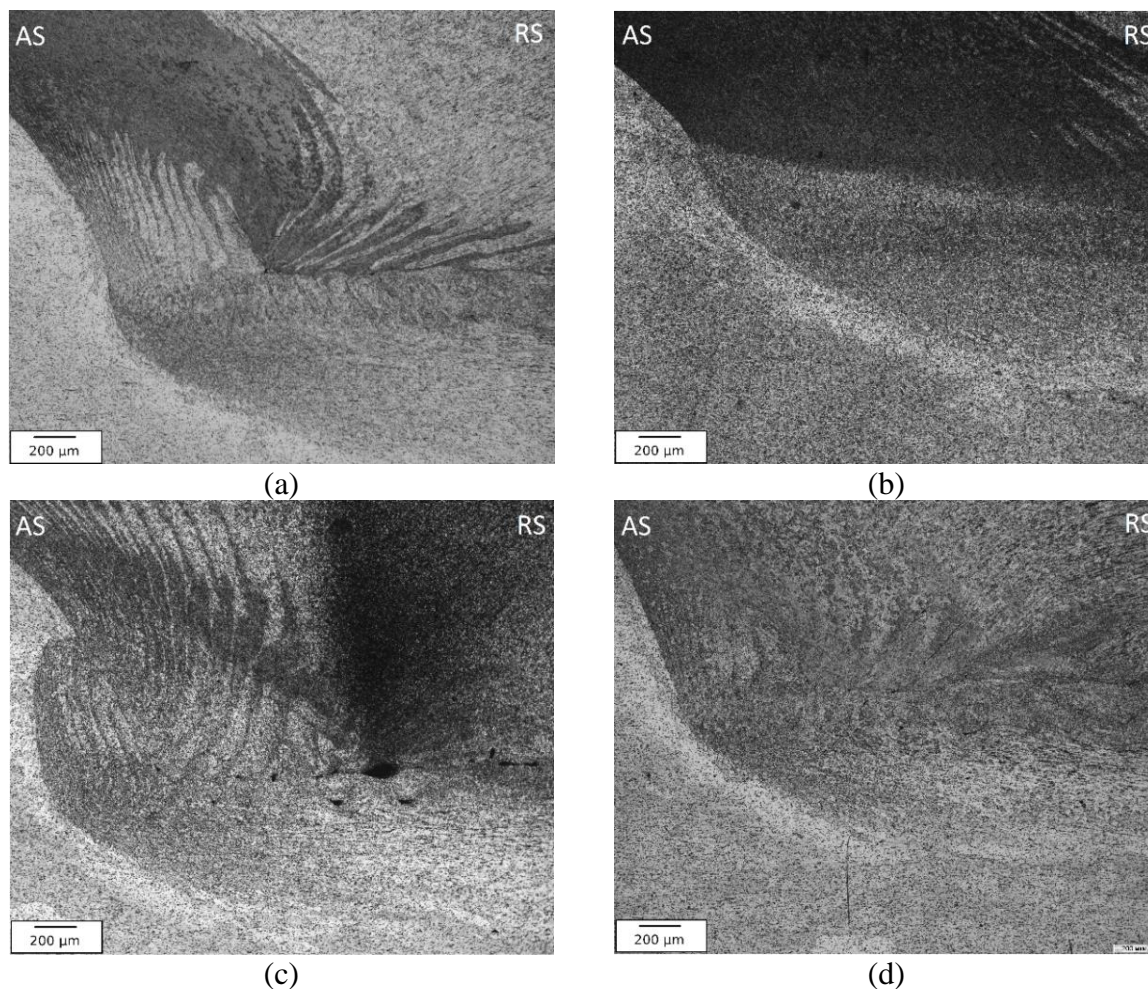


Fig. 4. The central part of the PZ in samples 205(a), 204 (b), 206 (c) and 207 (d), OM

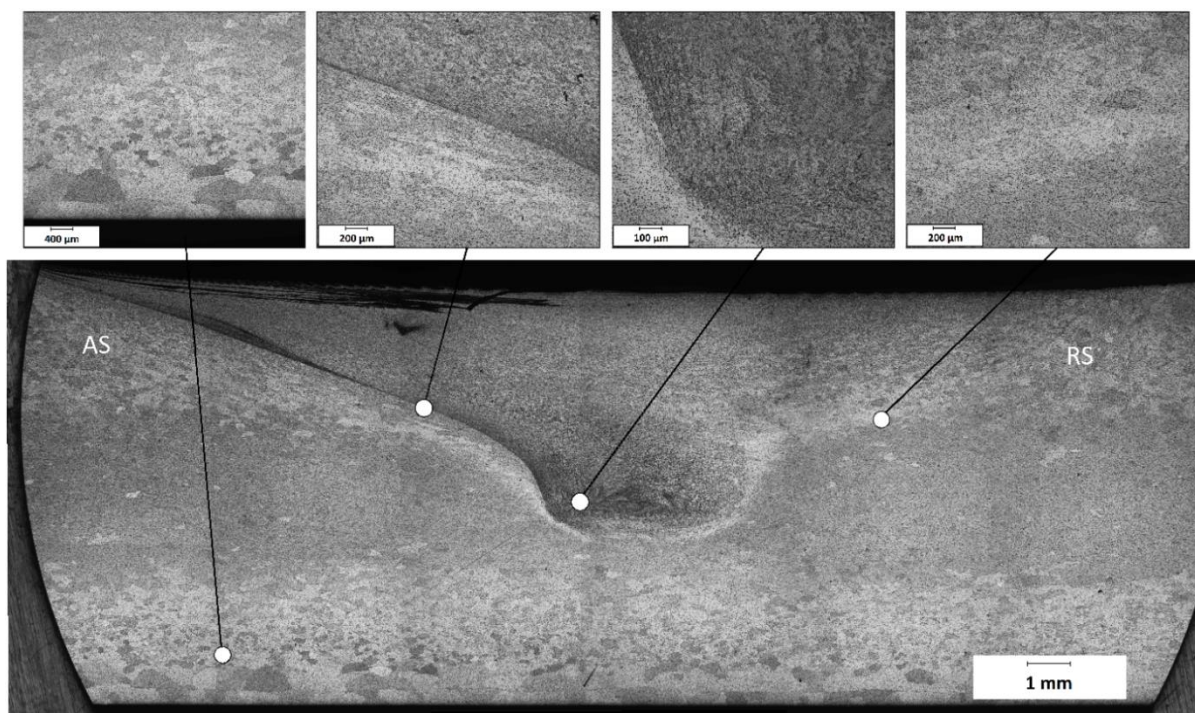


Fig. 5. Panoramic image of the microstructure of sample 207 after polishing and etching, OM

Figure 5 illustrates a panoramic image of the microstructure of sample 207. There is practically no transition layer between the SZ and the HAZ. The edge of the SZ is clearly visible. The slab of the base material is characterized by a heterogeneity of the structure over the cross section - at the surfaces (upper and lower) the grain size is large ($522 \pm 56 \mu\text{m}$), gradually decreasing towards the middle of the sample (from 324 to $53 \mu\text{m}$ with average size of $131 \pm 8 \mu\text{m}$); in the middle layer - fine, not detectable by etching. The similar microstructure could be observed in samples 205 and 206 as well. The difference in grain size throughout the sample, observed in the initial metallic plate, is the results of the quenching and natural aging.

Microstructure assessment. The sample 207 was previously characterized as the preferable from the absence of defects point of view. The microstructure of the sample 207 is presented on Fig. 6.

Intermetallic particles, presented in the material, don't have a significant impact on the structure and properties of the sample. According to Fig. 6(a-d) there is no notable difference in the size and morphology of the intermetallic particles before and after the FSP. The treatment, however, results in the decrease of the average grain/subgrain size within the PZ – from $274 \pm 22 \text{ nm}$ to $173 \pm 10 \text{ nm}$ (Fig. 6(e,f))

The presented experimental results show that in the FSP there is a significant refinement of the average grain size in the central region of the PZ, with the formation of a fine-grained equiaxed structure. The average grain size in the SZ decreases by a factor of 4–5 compared to the initial structure of the alloy (decreasing is more notable in the edges of the sample, where the initial grains are the largest).

The exact processes that occur during the FSP within the material structure are numerous and may happen simultaneously. Due to the combination of the high temperature and high deformation value within the SZ the dynamic recrystallization (both continuous and discontinuous), recovery, dislocation emission and annihilation, grain refinement take place. Usually, the structure of the material after FSP consists of the grain with the different degree of recrystallization and/or recovery place [13,24]. The exact combination of abovementioned mechanisms depends on the material and the FSP conditions, and to pinpoint each of them, the thorough structure analysis is required. However, in case of friction stir processing the processes on a microscale are not of an importance, since the presence/absence of macro defects has bigger value [8,25]. Since the recovery and recrystallization are inherent to the FSP, their presence might be used to an advantage – it is suggested that UFG materials could be subjected to FSP without loss of the UFG structure [9].

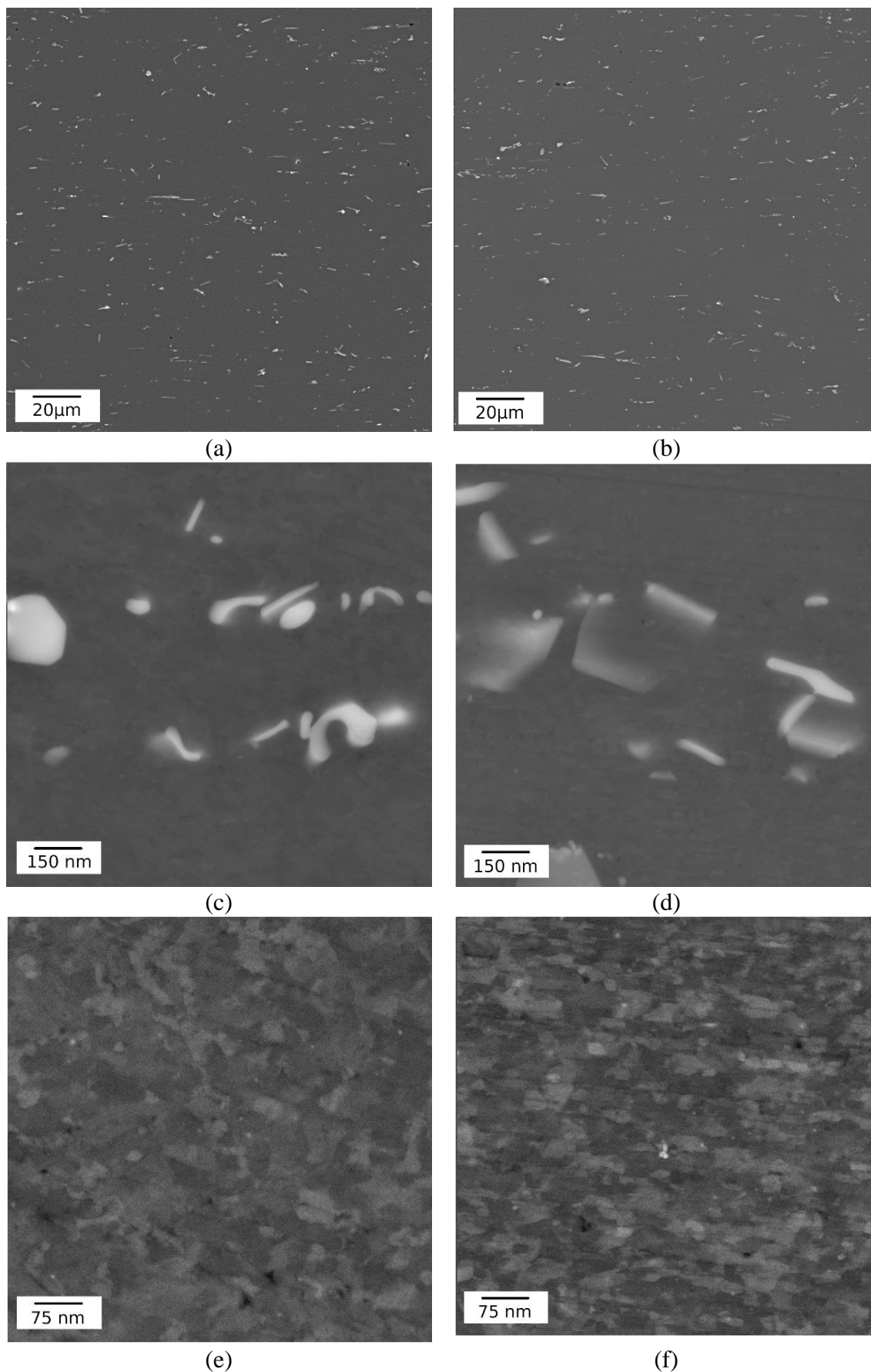


Fig. 6. Microstructure of the 207 sample: (a,c,e) – BM, (b,d,f) – SZ, SEM. Images a-d illustrate particles, e-f – grains/subgrains

Microhardness and electrical conductivity results. Figure 7 shows the obtained data on the distribution of microhardness over the cross section of the sample. For each sample three microhardness profiles were measured: at the bottom of the sample, in the middle and at the top.

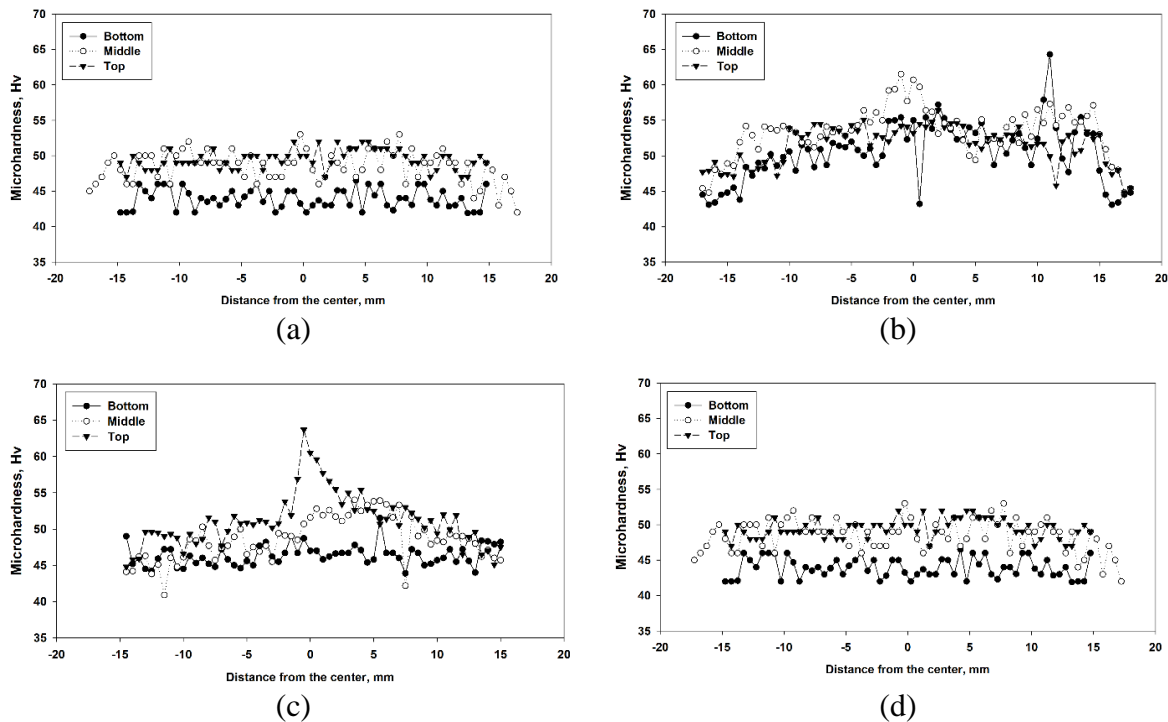


Fig. 7. Distribution of microhardness over the cross section of the samples 204 (a), 205 (b), 206 (c) and 207 (d). On all images the AS is on the right

The measurements showed that the microhardness values HV for all the samples under study are in the range of 40 – 65 HV. The middle profile is slightly higher for each of the samples due to the lower average grain size. Due to the uneven structure of the initial plate, there is no data for the microhardness of the BM, since it is different in different regions of the samples. At the same time, the microhardness profiles have tendency to rise (and even have a peak in sample 206) in the region of the PZ. The increase in microhardness is the result of grain boundary strengthening, which, in turn, is caused by a decrease in the average grain size in the SZ because of the thermomechanical treatment. It is noteworthy that the highest peak values of microhardness are observed in the sample obtained according to mode 206. Highest average microhardness values are demonstrated by the 205 sample.

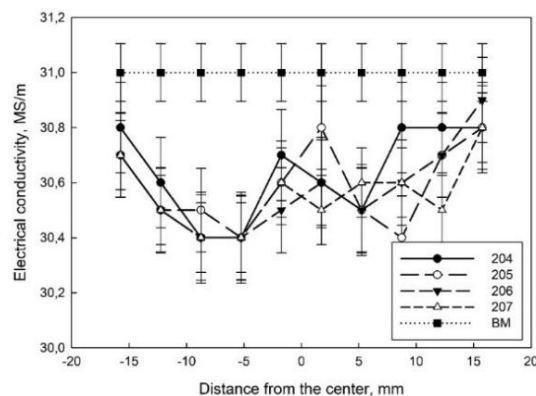


Fig. 8. Distribution of electrical conductivity over the cross section of the SZ in the samples 204-207. AS is on the right

Figure 8 shows the graphs of the distribution of the electrical conductivity of the investigated alloy after FSP. Since the electrical conductivity parameter is sensitive to structural defects, its change can be used to judge the homogeneity of the deformation.

Although all samples are characterized by a decrease in electrical conductivity in SZ relative to BM, associated with an increased density of structural defects, the difference in electrical conductivity values is relatively small and lies within the error value. Still, electrical conductivity measurements present the trend of electrical conductivity changes. The scatter of electrical conductivity values in samples 205 and 204 is higher than in samples 206 and 207, indicating a greater structural inhomogeneity in samples 205 and 204. All four samples are characterized by a local decrease in electrical conductivity in the first third of the sample, exactly where the transition zone between the BM and the HAZ is. From the point of view of the formation of a homogeneous structure within the PZ, mode 207 is optimal, which makes it possible to recommend it for further research.

The conducted studies of the relationship between the processing conditions of the FSP and the microstructure and properties of the obtained samples showed that with a decrease in the linear speed of the tool movement, the thermomechanical effect on the microstructure of the PZ increases noticeably. In the region of the PZ root, volumetric defects begin to be detected with a decrease in the linear speed of the tool. However, the size of these defects is relatively small, and continues to decrease with increasing linear speed of the tool. The importance of the macro defects within the stir zone cannot be overestimated – the presence of the crack or left by the FSP can lead to a premature failure of the material, nullifying all the attempts to increase the material's strength [8,17,25]. Thus, only after obtaining defectless structure, any further strength/performance attempts can be made.

The revealed patterns of structure formation during FSP and the tests carried out made it possible to select the technological parameters of the FSP, which provide both a decrease in the number and size of bulk defects and local hardening in the core. The proposed FSP mode can be transferred to other aluminum alloys.

The results obtained can be used for further work aimed at obtaining aluminum-based materials with modified structure and surface properties. Since the FSP conditions for the studied alloy were established, the different schemes of the FSP could be safely applied to this alloy. The further research is focused on providing the overlapping tracks [10–12], processing the material plate from both sides, doubling the processing routes [7].

Conclusions

1. The optimal technological parameters that ensure the formation of PZ with a relatively homogeneous defect-free structure with a small grain size at a given instrument geometry is a tool rotation frequency of 1120 rpm with a processing speed of 200 mm/min for the AD31T alloy.
2. An increase in the linear velocity of the stirring tool leads to a decrease in the heating temperature of the tool and the surrounding material and leads to a decrease of the HAZ. Since it is important not to overheat the material (to avoid recovery, oxidation, formation of a liquid phase and other undesirable processes) the increase in linear velocity of the tool not only decreases the treatment time, but also provides absence of the aforementioned defects.
3. Suggested FSP conditions provide the decrease of the electrical conductivity within the SZ by 2 % of the BM conductivity level without the loss of the microhardness, making this technique applicable to the installation of electric conductors.

References

1. Polmear I, StJohn D, Nie JF, Qian M. *Light Alloys: Metallurgy of the Light Metals*. 5th ed. Butterworth-Heinemann; 2017.
2. Verma RP, Kumar Lila M. A short review on aluminium alloys and welding in structural applications. *Mater. Today Proc.* 2021;46: 10687–10691.
3. Valiev RZ, Murashkin M, Sabirov I. A nanostructural design to produce high-strength Al alloys with enhanced electrical conductivity. *Scr. Mater.* 2014;76: 13–16.
4. Sabirov I, Murashkin MY, Valiev RZ. Nanostructured aluminium alloys produced by severe plastic deformation: New horizons in development. *Materials Science and Engineering A*. 2013;560: 1–24.
5. Christy JV, Mourad AHI, Sherif MM, Shivamurthy B. Review of recent trends in friction stir welding process of aluminum alloys and aluminum metal matrix composites. *Transactions of Nonferrous Metals Society of China (English Edition)*. 2021;31: 3281–3309.
6. Rambabu K, Gandhi P, Susmitha M, Sravanthi K. A review on different techniques to produce gradient structured material. *Mater. Today Proc.* 2022;60: 2262–2265.
7. Nicholas ED. Friction Processing Technologies. *Welding in the World*. 2003;47: 2–9.
8. Manjhi SK, Das A, Prasad SB. Review on joining of aluminum alloy by solid-state welding technique. *Mater. Today Proc.* 2020;26: 1255–1261.
9. Vysotskii I, Malopheyev S, Mironov S, Kaibyshev R. Deformation behavior of friction-stir welded Al-Mg-Mn alloy with ultrafine-grained structure. *Mater. Charact.* 2022;185: 111758.
10. Su JQ, Nelson TW, Sterling CJ. Friction stir processing of large-area bulk UFG aluminum alloys. *Scr. Mater.* 2005;52: 135–140.
11. Su JQ, Nelson TW, Sterling CJ. Microstructure evolution during FSW/FSP of high strength aluminum alloys. *Materials Science and Engineering A*. 2005;405: 277–286.
12. Su JQ, Nelson TW, Sterling CJ. A new route to bulk nanocrystalline materials. *Journal of Materials Research*. 2003;18: 1757–1760.
13. Yadav D, Bauri R. Effect of friction stir processing on microstructure and mechanical properties of aluminium. *Materials Science and Engineering A*. 2012;539: 85–92.
14. Mimmi A, Merzoug M, Ghazi A, Dellal N. Mechanical behavior of structures welded with friction stir lap welding process. *Materials Physics and Mechanics*. 2023;51: 151–163.
15. Liyakat NA, Veeman D. Improvement of mechanical and microstructural properties of AA 5052-H32 TIG weldment using friction stir processing approach. *Journal of Materials Research and Technology*. 2022;19: 332–344.
16. Sarmadi H, Kokabi AH, Seyed Reihani SM. Friction and wear performance of copper-graphite surface composites fabricated by friction stir processing (FSP). *Wear*. 2013;304: 1–12.
17. Sharma V, Gupta Y, Kumar BVM, Prakash U. Friction Stir Processing Strategies for Uniform Distribution of Reinforcement in a Surface Composite. *Materials and Manufacturing Processes*. 2016;31: 1384–1392.
18. Sharma A, Khan ZA, Siddiquee AN. A short review of the effect of plunge depth on friction stir welding of aluminium pipes. *Mater. Today Proc.* 2022;64: 1504–1506.
19. Isa MSM, Moghadasi K, Ariffin MA, Raja S, bin Muhamad MR, Yusof F, Jamaludin MF, Yusoff N, Ab Karim MS. Recent research progress in friction stir welding of aluminium and copper dissimilar joint: a review. *Journal of Materials Research and Technology*. 2021;15: 2735–2780.
20. Singh VP, Patel SK, Ranjan A, Kuriachen B. Recent research progress in solid state friction-stir welding of aluminium–magnesium alloys: a critical review. *Journal of Materials Research and Technology*. 2020;9: 6217–6256.
21. Mishra RS, De PS, Kumar N. Friction Stir Processing. *Friction Stir Welding and Processing*. Springer; 2014. p.259–96.

22. Memon S, Paidar M, Ojo OO, Cooke K, Babaei B, Masoumnezhad M. The role of stirring time on the metallurgical and mechanical properties during modified friction stir clinching of AA6061-T6 and AA7075-T6 sheets. *Results Phys.* 2020;19: 103364.
23. Wakchaure K, Thakur A. Mechanical and microstructural characteristics of underwater friction stir welded AA 6061-T6 joints using a hybrid GRA-artificial neural network approach. *Materials Physics and Mechanics.* 2023;51: 119–141.
24. Bauri R, Yadav D, Suhas G. Effect of friction stir processing (FSP) on microstructure and properties of Al-TiC in situ composite. *Materials Science and Engineering A.* 2011;528: 4732–4739.
25. Kumar N, Das A. Ecofriendly energy efficient welding of aluminium matrix composites for aerospace applications: A state of art review. *Mater. Today Proc.* 2020;26: 1666–1675.

THE AUTHORS

Medvedev A.E. 

e-mail: medvedevandreyrf@gmail.com

Selivanov A.S.

e-mail: selivanov@naks-rb.ru

Gorbatkov M.V.

e-mail: m.gorbatkov@krus-zapad.ru

Lobachev V.S.

e-mail: vladik1997okt@mail.ru

Atroshchenko V.V.

e-mail: 91250@mail.ru

Bogdanov A.R.

e-mail: bogdanov-alb02@mail.ru

Logachev Y.V.

e-mail: logachev.sts@mail.ru

Sadrislamov A.R.

e-mail: artem22sad@gmail.com